

Cognitive Radar Antenna Selection via Deep Learning

Ahmet M. Elbir¹, Kumar Vijay Mishra^{2*}, Yonina C. Eldar²

¹ Department of Electrical and Electronics Engineering, Duzce University, Duzce, Turkey

² Andrew and Erna Viterbi Faculty of Electrical Engineering, Technion-Israel Institute of Technology, Haifa, Israel

* E-mail: mishra@ee.technion.ac.il

ISSN 1751-8644

doi: 0000000000

www.ietdl.org

arXiv:1802.09736v1 [eess.SP] 27 Feb 2018

Abstract: Direction of arrival (DoA) estimation of targets improves with the number of elements employed by a phased array radar antenna. Since larger arrays have high associated cost, area and computational load, there is recent interest in thinning the antenna arrays without loss of far-field DoA accuracy. In this context, a cognitive radar may deploy a full array and then select an optimal subarray to transmit and receive the signals in response to changes in the target environment. Prior works have used optimization and greedy search methods to pick the best subarrays cognitively. In this paper, we leverage deep learning to address the antenna selection problem. Specifically, we construct a convolutional neural network (CNN) as a multi-class classification framework where each class designates a different subarray. The proposed network determines a new array every time data is received by the radar, thereby making antenna selection a cognitive operation. Our numerical experiments show that the proposed CNN structure outperforms existing random thinning and other machine learning approaches.

1 Introduction

Cognitive radar has gained much attention in the last decade due to its ability to adapt both the transmitter and receiver to changes in the environment and provide flexibility for different scenarios as compared to conventional radar systems [1–3]. Several applications have been considered for radar cognition such as waveform design [4–7], target detection and tracking [8, 9], spectrum sensing and sharing [10, 11]. Cognitive radar design requires reconfigurable circuitry for many subsystems such as power amplifiers, waveform generator, and antenna arrays [12]. In this paper, we focus on this latter aspect of antenna array design in cognitive radar.

For a given wavelength, good angular resolution is achieved by a wide array aperture resulting in a large number of array elements, physical area and the cost associated with the array circuitry [13–15]. Hence, general approaches have been proposed to effectively use the array output with minimal number of antenna elements. For example, non-uniform array structures [16, 17] are used to virtually increase the array aperture for direction-of-arrival (DoA) estimation. Given a full Nyquist antenna array, one could also randomly choose a few antenna elements to transmit/receive (Tx/Rx) and then employ efficient recovery algorithms so that the spatial resolution does not degrade [13, 18, 19]. However, such approaches are agnostic to information about the received signal. A cognitive approach may be to select these Tx/Rx antennas based on the current target scenario encoded in the received signal [12] connecting antenna selection with contemporary interest in cognitive radar. The key idea is to exploit available data from the current radar scan to choose an optimal subarray for the next scan since target locations change little during consecutive scans.

Recent research [20, 21] has proposed a reconfigurable array structure for a cognitive radar which obtains an adaptive switching matrix after a combinatorial search for an optimal subarray that minimizes a lower bound on the DoA estimation error. A related work in [22] proposed a greedy search algorithm to find a subarray that maximizes the mutual information between the collected measurements and the far-field array pattern. Very recently, a semidefinite program proposed in [23] selects a Tx-Rx antenna pair for a multiple-input-multiple-output (MIMO) radar that maximizes the separation between desired and parasitic DoAs. Similar problems have also been investigated in communications especially in

the context of massive MIMO [24] to achieve energy and cost efficient antenna designs and beamforming [25–27]. More generally, in the context of sensor selection, [28, 29] solve convex optimization problems to obtain optimal antenna subarrays for DoA estimation. Similarly, [30] selects the sensors for a distributed multiple-radar scenario through greedy search with the Cramér-Rao lower bound (CRB) as a performance metric.

Nearly all of these formulations solve a mathematical optimization problem or use a greedy search algorithm. A few other works explore supervised machine learning (ML) to estimate DoA in the context of radar [31] and communications [32, 33]. Specifically, [34] employs support vector machines (SVM) for antenna selection in wireless communications. As a class of ML methods, deep learning (DL) has gained much interest recently for the solution of many challenging problems such as speech recognition, visual object recognition, and language processing [35, 36]. DL has several advantages such as low computational complexity when solving optimization-based or combinatorial search problems and the ability to extrapolate new features from a limited set of features contained in a training set [32, 35]. In the context of radar, DL has found applications in waveform recognition [37], image classification [38, 39] and range-Doppler signature detection [40].

In this paper, we introduce a DL-based approach for antenna selection in a cognitive radar. DL approaches directly fit our setting because the antenna selection problem can be considered as a classification problem where each subarray designates a class. Among prior studies, the closest to our work is [34] where SVM is fed with the channel state information (CSI) to select subarrays for the best MIMO communication performance. However, SVM is not as powerful as DL for extracting feature information inherit in the input data [35]. Furthermore, [34] considers only small array sizes. On the other hand, the optimization methods suggested in [29, 30] assume *a priori* knowledge of the target location/DoA angle to compute the CRB. Compared to these studies, we leverage DL to consider a relatively large scale of the selection problem wherein the feature maps can be extracted to train the network for different array geometries. The proposed approach avoids solving a difficult optimization problem [28]. Unlike random array thinning where a fixed subarray is used for all scans, we select a new subarray based on the received data. In contrast to [29, 30], we also assume that the target DoA angle is unknown while choosing the array elements. To the best of

our knowledge, this is the first work that addresses the radar antenna selection problem using DL.

In particular, we construct a convolutional neural network (CNN) for our problem. The input data to our CNN are the covariance samples of the received array signal. Previous radar DL applications [37–40] have used image-like inputs such as synthetic aperture radar signatures and time-frequency spectrograms. Our proposed CNN models the selection of K best antennas out of M as a classification problem wherein each class denotes an antenna subarray. In order to create the training data, we choose those subarrays which estimate DoA with the lowest minimal bound on the mean-squared-error (MSE). We consider minimization of CRB as the performance benchmark in generating training sets for 1-D uniform linear arrays (ULA) and 2-D geometries such as uniform circular arrays (UCA) and randomly deployed arrays (RDA). For ULAs, we also train the network with data obtained by minimizing Bayesian bounds such as the Bobrovsky-Zakai bound (BZB) and Weiss-Weinstein bound (WWB) on DoA [41] because these bounds provide better estimates of MSE at low signal-to-noise-ratios (SNRs). In particular BZB-based selection has been shown to have the ability to control the sidelobes and avoid ambiguity in DoA estimation [20, 21].

The rest of the paper is organized as follows. In the next section, we describe the system model and formulate the antenna selection problem. In Section 3, we introduce the proposed CNN and provide details on the training data. We evaluate the performance of our DL method in Section 4 through several numerical experiments.

Throughout the paper, we reserve boldface lowercase and uppercase letters for vectors and matrices, respectively. The i th element of a vector \mathbf{y} is $y(i)$ while the (i, j) th entry of the matrix \mathbf{Y} is $[\mathbf{Y}]_{i,j}$. We denote the transpose and Hermitian by $(\cdot)^T$ and $(\cdot)^H$, respectively. The functions $\angle\{\cdot\}$, $\Re\{\cdot\}$ and $\Im\{\cdot\}$ designate the phase, real and imaginary parts of a complex argument, respectively. The combination of selecting K terms out of M is denoted by $\binom{M}{K} = \frac{M!}{K!(M-K)!}$. The calligraphic letters \mathcal{S} and \mathcal{L} denote the position sets of all and selected subarrays respectively. The Hadamard (point-wise) product is written as \odot . The functions $E\{\cdot\}$ and \max give the statistical expectation and maximum value of the argument, respectively. The notation $x \sim \mathcal{U}\{[u_l, u_u]\}$ means a random variable drawn from the uniform distribution over $[u_l, u_u]$ and $x \sim \mathcal{CN}(\mu_x, \sigma_x^2)$ represents the complex normal distribution with mean μ_x and variance σ_x^2 .

2 System Model and Problem Formulation

Consider a phased array antenna with M elements where each element transmits a pulsed waveform $s(t)$ towards a Swerling Case 1 point target. Since we are interested only in DoA recovery, the range and Doppler measurements are not considered and target's complex reflectivity is set to unity. We characterize the target through its DoA $\Theta = (\theta, \phi)$ where θ and ϕ denote, respectively, the elevation and the azimuth angles with respect to the radar. The radar's pulse repetition interval and operating wavelength are, respectively, T_s and $\lambda = c_0/f_0$, where $c_0 = 3 \times 10^8 \text{ ms}^{-1}$ is the speed of light and $f_0 = \omega_0/2\pi$ is the carrier frequency.

To further simplify the geometries, we suppose that the targets are far enough from the radar so that the received signal wavefronts are effectively planar over the array. The array receives a narrowband signal reflected from a target located in the far-field of the array at Θ . We denote the position vector of the m th receive antenna by $\mathbf{p}_m = [p_{x_m}, p_{y_m}, p_{z_m}]^T$ and assume that the antennas are identical and well calibrated.

Let $s(t)$ and $y_m(t)$ denote the source signal and the output signal at the m th sensor of the array, respectively. The baseband continuous-time received signal at the m th antenna is then

$$y_m(t) = a_m(\Theta)s(t) + n_m(t), \quad 0 \leq t \leq T_s, \quad (1)$$

where $n_m(t)$ is temporally and spatially white zero-mean Gaussian noise with variance σ_n^2 and

$$a_m(\Theta) = \exp \left\{ j \frac{2\pi}{\lambda} c_0 \tau_m \right\}, \quad (2)$$

is the m th element of the steering vector

$$\mathbf{a}(\Theta) = [a_1(\Theta), a_2(\Theta), \dots, a_M(\Theta)]^T. \quad (3)$$

Here, τ_m is the time delay from the target to the m th antenna, and is given by $\tau_m = -\frac{1}{c_0} \mathbf{p}_m^T \mathbf{r}(\Theta)$ where $\mathbf{r}(\Theta)$ is the 2-D DoA parameter

$$\mathbf{r}(\Theta) = [\cos(\phi) \sin(\theta), \sin(\phi) \sin(\theta), \cos(\theta)]^T. \quad (4)$$

Suppose the radar acquires the signal for L snapshots at time T . For a given snapshot l , we define an $M \times 1$ received signal vector $\mathbf{y}(lT) = [y_1(lT), \dots, y_M(lT)]^T$. For all L snapshots and omitting T from the indices for notational simplicity, we can express the received signal in matrix form as

$$\mathbf{Y} = \mathbf{a}(\Theta) \mathbf{s}^T + \mathbf{N}, \quad (5)$$

where $M \times L$ matrix $\mathbf{Y} = [\mathbf{y}(1), \dots, \mathbf{y}(L)]$, $\mathbf{s} = [s(1), \dots, s(L)]^T$, and $\mathbf{N} = [\mathbf{n}(1), \dots, \mathbf{n}(L)]$ with $\mathbf{n}(l) = [n_1(l), \dots, n_M(l)]^T$ the noise term. We assume that the possible target locations lie on a grid of G points $\tilde{\Theta}_{1:G}$ such that $\Theta = \tilde{\Theta}_i$ for some $i \in \{1, \dots, G\}$.

Expanding the inner product $\mathbf{p}_m^T \mathbf{r}(\Theta)$ in the array steering vector gives $a_m(\Theta) = \exp \left\{ j \frac{2\pi}{\lambda} (p_{x_m} \mu + p_{y_m} \nu + p_{z_m} \xi) \right\}$, where $\mu = \cos(\phi) \sin(\theta)$, $\nu = \sin(\phi) \sin(\theta)$, and $\xi = \cos(\theta)$. Evidently, $a_m(\Theta)$ is a multi-dimensional harmonic. Once the frequencies μ , ν , and ξ in different directions are estimated, the DoA angles are obtained using the relations

$$\theta = \tan^{-1} \left(\frac{\nu}{\mu} \right), \quad \phi = \cos^{-1} \left(\frac{\xi}{\sqrt{\mu^2 + \nu^2 + \xi^2}} \right), \quad (6)$$

with the usual ambiguity in $[0, 2\pi]$. In case of a linear array, there is only one parameter in the steering vector whereas two parameters are involved in planar and three-dimensional arrays.

For instance, consider a planar array so that $p_{z_m} = 0$ and there is only one incoming wave. Then, a minimal configuration to find the two frequencies consists of at least three elements in an L-shape configuration to estimate frequencies in the x - and y -directions. More sensors are needed if the incoming signal is a superposition of P wavefronts. Many theoretical works have investigated the uniqueness of 2-D harmonic retrieval (see e.g., [42–44]). For example, in case of a uniform rectangular array of size $M_1 \times M_2$, classically $P \leq M_1 M_2 - \min(M_1, M_2)$ specifies the minimum required number of sensors in the absence of noise. This can be relaxed by obtaining several snapshots or using coprime sampling if the sources are uncorrelated [16, 17] or spatial compressed sensing [18, 19].

In the antenna selection scenario, the radar has M antennas but desires to use only $K < M$ elements to save computational cost, energy and sharing aperture momentarily to look at other directions. In practice, the signal is corrupted with noise and the antenna elements are not ideally isotropic. Therefore, K should be larger than the minimum elements predicted by classical results. Removal of elements from an array raises the sidelobe levels and introduces ambiguity in resolving DoA. The exact choice of K depends on the estimation algorithm employed by the receiver processor. For example, [18, 19, 44] provide different guarantees for the minimum K depending on the array configuration and algorithm used for extracting the DoA.

In general, the target's position changes little during consecutive scans while a phased array can switch very fast from one antenna configuration to the other. Our goal is to use the received signal from the current scan and find an optimal antenna array for the next scan. This switching of elements between different scans is a cognitive operation because a new array is determined every time the radar receives echoes from the target scene. In the next section, we describe our DL approach to cognitive antenna selection.

3 Deep Neural Network for Antenna Selection

Assume that an antenna subarray composed of K antennas is to be selected from an M -element antenna array. There are $Q = \binom{M}{K}$ possible choices. This can be viewed as a classification problem with Q classes each of which represents a different subarray. Let $\mathcal{P}_k^q = \{p_{x_k}^q, p_{y_k}^q, p_{z_k}^q\}$, $k = 1, \dots, K$, be the set of the k th antenna

coordinates in the q th subarray. Then, the q th class consisting of the positions of all elements in the q th subarray is

$$\mathcal{S}_q = \{\mathcal{P}_1^q, \dots, \mathcal{P}_K^q\}, \quad (7)$$

and all classes are given by the set

$$\mathcal{S} = \{\mathcal{S}_1, \mathcal{S}_2, \dots, \mathcal{S}_Q\}. \quad (8)$$

In Section 3.2, we propose a CNN to solve this classification problem. To train the network, we discuss in Section 3.1 our procedure to create training data relying on the CRB. Note that, for an operational radar, generation of an artificial or simulated dataset to train the DL network is not necessary. Instead, the network can train itself with the data acquired by the radar during previous scans. During the test phase, for which we present results in Section 4, the DoA angles are unknown to the network. The CNN accepts the features from the estimated covariance matrix and outputs a new array. This stage is, therefore, cognitive because the radar is adapting the antenna array in response to the received signal.

3.1 Training Data Design

The training samples are the input for the CNN. In order to generate the training data, we select a set of target DoA locations and analyze all possible array configurations. We then generate class labels for those arrays that minimize a lower-bound on the DoA estimation error. We choose CRB to label the training samples because this bound leads to simplified expressions. However, other bounds can also be considered [20, 21, 34, 45].

Consider L statistically independent observations of the q th subarray with K elements

$$\mathbf{y}_q(l) = \mathbf{a}_q(\Theta) s(l) + \mathbf{n}_q(l), \quad (9)$$

where $\mathbf{a}_q(\Theta)$ and $\mathbf{n}_q(l)$ denote the $K \times 1$ elements of $\mathbf{a}(\Theta)$ and $\mathbf{n}(l)$ corresponding to the q th subarray position set \mathcal{S}_q . The signal and noise are assumed to be stationary and ergodic over the observation period. The covariance matrix of the observations for the q th subarray is

$$\mathbf{R}_q = \mathbb{E} \left\{ \mathbf{y}_q \mathbf{y}_q^H \right\} = \mathbf{a}_q(\Theta) \mathbb{E} \{ s[l] s^H[l] \} \mathbf{a}_q^H(\Theta) + \sigma_n^2 \mathbf{I}_K, \quad (10)$$

where \mathbf{I}_K is the identity matrix of dimension K . In order to simplify the CRB expressions, we represent $K \times 1$ steering vector $\mathbf{a}_q(\Theta)$ as \mathbf{a}_q , and assume that $\mathbb{E} \{ s[l] s^H[l] \} = \sigma_s^2$ and σ_n^2 are known. For this model, the CRBs for jointly estimating the target DoA coordinates θ and ϕ are, respectively, [46–48]

$$\text{CRB}_\theta = \frac{\sigma_n^2}{2L \operatorname{Re} \{ (\dot{\mathbf{a}}_{q\theta}^H [\mathbf{I}_K - \mathbf{a}_q \mathbf{a}_q^H / K] \dot{\mathbf{a}}_{q\phi}) \odot (\sigma_s^4 \mathbf{a}_q^H \mathbf{R}_q^{-1} \mathbf{a}_q) \}}, \quad (11)$$

and

$$\text{CRB}_\phi = \frac{\sigma_n^2}{2L \operatorname{Re} \{ (\dot{\mathbf{a}}_{q\phi}^H [\mathbf{I}_K - \mathbf{a}_q \mathbf{a}_q^H / K] \dot{\mathbf{a}}_{q\theta}) \odot (\sigma_s^4 \mathbf{a}_q^H \mathbf{R}_q^{-1} \mathbf{a}_q) \}}. \quad (12)$$

The partial derivatives $\dot{\mathbf{a}}_{q\theta} = \frac{\partial \mathbf{a}_q}{\partial \theta}$ and $\dot{\mathbf{a}}_{q\phi} = \frac{\partial \mathbf{a}_q}{\partial \phi}$ are computed using the expressions in (2)–(3). The absolute CRB [48] for the two-dimensional DoA $\Theta = \{\theta, \phi\}$ using subarray \mathcal{S}_q is

$$\eta(\Theta, \mathcal{S}_q) = \frac{1}{\sqrt{2}} (\text{CRB}_\theta^2 + \text{CRB}_\phi^2)^{1/2}. \quad (13)$$

In order to label the training samples, we compute the CRB $\eta(\Theta, \mathcal{S}_q)$ for each target direction Θ in the training set with all subarrays $q = 1, \dots, Q$. We then produce class labels for the input data to indicate the *best array*, i.e. the array which minimizes the CRB in a given scenario. Let us define \bar{Q} as the number of subarrays that provide the best DoA estimation performance for different directions. Then, \bar{Q} is generally much smaller than Q because of the direction of the target and the aperture of the subarrays. For an illustrative comparison of Q and \bar{Q} , we refer the reader to Table 1 which lists the

Table 1 Number of classes Q and the reduced number of classes \bar{Q} for the uniform circular array (UCA) geometry with $M = 10$ and $M = 16$ antennas. Here, elevation angle is fixed at $\theta = 90^\circ$ and the number of azimuthal grid points $P_\phi = 10000$ for uniformly gridded azimuth plane in $[0^\circ, 360^\circ]$.

	$K = 3$	$K = 4$	$K = 5$	$K = 6$	$K = 7$	$K = 8$
			UCA with $M = 10$			
Q	120	210	252	210	120	45
\bar{Q}	10	10	10	10	10	9
			UCA with $M = 16$			
Q	560	1820	4368	8008	11440	12870
\bar{Q}	16	10	16	11	16	16

numbers of these classes for a uniform circular array. Hence, we construct a new set \mathcal{L} which includes only those classes that represent the selected subarrays for different directions

$$\mathcal{L} = \{l_1, l_2, \dots, l_{\bar{Q}}\}, \quad (14)$$

where \bar{Q} is the reduced number of classes: $l_{\bar{Q}}$ is the subarray class that provides the lowest CRB and for direction Θ , namely

$$l_{\bar{Q}} = \arg \min_{q=1, \dots, Q} \eta(\Theta, \mathcal{S}_q), \quad (15)$$

for $\bar{q} = 1, \dots, \bar{Q}$. Once the label set \mathcal{L} is obtained, the input-output data pairs are constructed as (\mathbf{R}_q, z) where $z \in \mathcal{L}$ is the output label which represents the best subarray index for the covariance input \mathbf{R}_q .

We summarize the steps for generating the training data in Algorithm 1. In Step 4 of the Algorithm, the class \mathcal{L} is chosen from the full combination \mathcal{Q} . For large size arrays, one could train by choosing less correlated subarrays or even randomly dropping out some of the subarrays. The covariance matrix used in the computation of the CRB in step 4 is the sample data covariance $\hat{\mathbf{R}}_q = \frac{1}{L} \sum_{l=1}^L \mathbf{y}_q(l) \mathbf{y}_q^H(l)$. Even though an analytical expression for \mathbf{R}_q is available, we use the sample data covariance here because it is closer to a practical radar operation where, in general, \mathbf{R}_q is estimated.

Algorithm 1 Training data generation.

Input: Number of given antenna elements M , number of desired elements K , number of snapshots L , number of different DoA angles considered P , number of signal and noise realizations T .

Output: Training data: Input-output pairs consisting of sample covariances $\hat{\mathbf{R}}_q^{(i,p)}$ and output labels $z_p^{(i)}$ for $p = 1, \dots, P$ and $i = 1, \dots, T$.

- 1: Select P DoA angles $\Theta_p = (\theta_p, \phi_p)$ for $p = 1, \dots, P$.
- 2: Generate T different realizations of the array output $\{\mathbf{Y}_p^{(i)}\}_{i=1}^T$ for $p = 1, \dots, P$ as

$$\mathbf{Y}_p^{(i)} = [\mathbf{y}_p^{(i)}(1), \dots, \mathbf{y}_p^{(i)}(L)],$$

where $\mathbf{y}_p^{(i)}(l) = \mathbf{a}(\Theta_p) s^{(i)}(l) + \mathbf{n}^{(i)}(l)$, $s^{(i)}(l) \sim \mathcal{CN}(0, \sigma_s^2)$ and $\mathbf{n}^{(i)}(l) \sim \mathcal{CN}(0, \sigma_n^2 \mathbf{I})$.

- 3: Construct the input data $\hat{\mathbf{R}}_q^{(i,p)}$.
- 4: Compute the CRB values $\eta(\Theta_p, \mathcal{S}_q)$ following (13) and obtain the class set \mathcal{L} representing the best subarrays using (15).
- 5: Generate the input-output pairs as $(\hat{\mathbf{R}}_q^{(i,p)}, z_p^{(i)})$ for $p = 1, \dots, P$ and $i = 1, \dots, T$.
- 6: Construct training data by concatenating the input-output pairs:

$$\mathcal{D}_{\text{train}} = \{(\hat{\mathbf{R}}_q^{(1,1)}, z_1^{(1)}), (\hat{\mathbf{R}}_q^{(2,1)}, z_1^{(2)}), \dots, (\hat{\mathbf{R}}_q^{(T,1)}, z_1^{(T)}), (\hat{\mathbf{R}}_q^{(1,2)}, z_2^{(1)}), \dots, (\hat{\mathbf{R}}_q^{(T,P)}, z_P^{(T)})\},$$

where the size of the training dataset is $J = TP$.

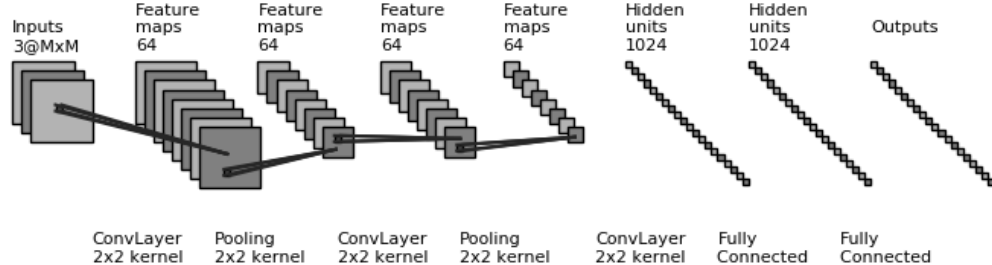


Fig. 1. The structure of the CNN for antenna selection.

3.2 Network Structure and Training

Using the labeled training dataset, we build a trained CNN classifier. The input of this learning system is the data covariance and the output is the index of the selected antenna set.

Given the $M \times L$ output \mathbf{Y} of the antenna array, the corresponding sample covariance is a complex-valued $M \times M$ matrix $\hat{\mathbf{R}}$. The first step towards efficient classification is to define a set of real-valued features that capture the distinguishing aspects of the output. The features we consider in this work are the angle, real and imaginary parts of \mathbf{R} . One could also consider magnitude here but we did not find much difference in the results when this feature was included. We construct three $M \times M$ real-valued matrices $\{\mathbf{X}_c\}_{c=1}^3$ whose (i, j) th entry contain, respectively, the phase, real and imaginary parts of the signal covariance matrix \mathbf{R} : $[\mathbf{X}_1]_{i,j} = \angle[\mathbf{R}]_{i,j}$; $[\mathbf{X}_2]_{i,j} = \text{Re}\{\mathbf{R}_{i,j}\}$; and $[\mathbf{X}_3]_{i,j} = \text{Im}\{\mathbf{R}_{i,j}\}$.

Figure 1 depicts the deep learning CNN structure that we used. The proposed network consists of 9 layers. In the first layer, the CNN accepts the two-dimensional inputs $\{\mathbf{X}_c\}_{c=1}^3$ in three real-valued channels. The second, fourth and sixth layers are convolutional layers with 64 filters of size 2×2 . The third and fifth layers are max-pooling to reduce the dimension by 2. The seventh and eighth layers are fully connected with 1024 units whose 50% are randomly dropped out to reduce overfitting in training [49]. There are rectified linear units (ReLU) after each convolutional and fully connected layers where the $\text{ReLU}(x) = \max(x, 0)$. At the output layer, there are Q units wherein the network classifies the given input data using a softmax function and reports the probability distribution of the classes to provide the best subarray.

In order to train the proposed CNN, we sample the target space for different directions and collect the data for several realizations. We realized the proposed network in MATLAB on a PC with 768-core GPU. During the training process, 90% and 10% of all data generated are selected as the training and validation datasets, respectively. Validation aids in hyperparameter tuning during the training phase to avoid the network simply memorizing the training data rather than learning general features for accurate prediction with new (test) data. We used the stochastic gradient descent algorithm with momentum [50] for updating the network parameters with learning rate 0.05 and mini-batch size of 500 samples for 50 epochs. As a loss function, we use the negative log-likelihood or cross-entropy loss. Another useful metric we consider for evaluating the network is the accuracy:

$$\text{Accuracy (\%)} = \frac{\zeta}{J} \times 100, \quad (16)$$

where J is the total number of input datasets in which the model identified the best subarrays correctly ζ times. This metric is available for training, validation and test phases.

4 Numerical Experiments

In this section, we present numerical experiments to train and test the proposed CNN structure shown in Fig. 1 for different antenna

geometries. In the following, we append subscripts TEST and TRAIN to indicate parameter values used for training and testing modes, respectively.

4.1 Uniform Linear Array

We first analyze the effect of the performance metrics on the antenna selection and DoA estimation accuracy by employing the simplest and most common geometry of a uniform linear array (ULA). For creating the training data, we employed three bounds: CRB, BZB and WWB [41]. The network was trained for $M = 10$, $K = 4$, $L_{\text{TRAIN}} = 100$ snapshots, $T_{\text{TRAIN}} = 100$ signal and noise realizations, and $P_{\text{TRAIN}} = 100$ DoA angles. The number of uniformly spaced azimuthal grid points are set to $P_\phi = 10000$.

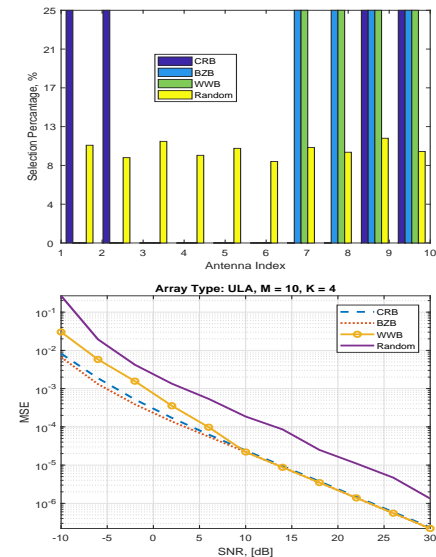


Fig. 2 Top: Antenna selection percentage over $J_{\text{TEST}} = 10000$ trials. Bottom: MSE of DoA for selected subarrays. The array geometry is ULA with $M = 10$ and $K = 4$.

For test mode, we fed the network with data corresponding to $P_{\text{TEST}} = 100$ DoA angles different than the ones used in the training phase but keeping the values of M , K , L and T same as in the training. The top plot of Fig. 2 shows the percentage of times a particular antenna index appears as part of the optimal array in the output over $J_{\text{TEST}} = T_{\text{TEST}} P_{\text{TEST}}$ trials with different performance metrics used during training. As seen here, when CNN is trained with data created from the CRB, the classifier output arrays usually consists of the elements at the extremities. However, the network trained on BZB and WWB usually selects arrays with elements close to each other leading to low sidelobe levels. Also shown here is the random selection

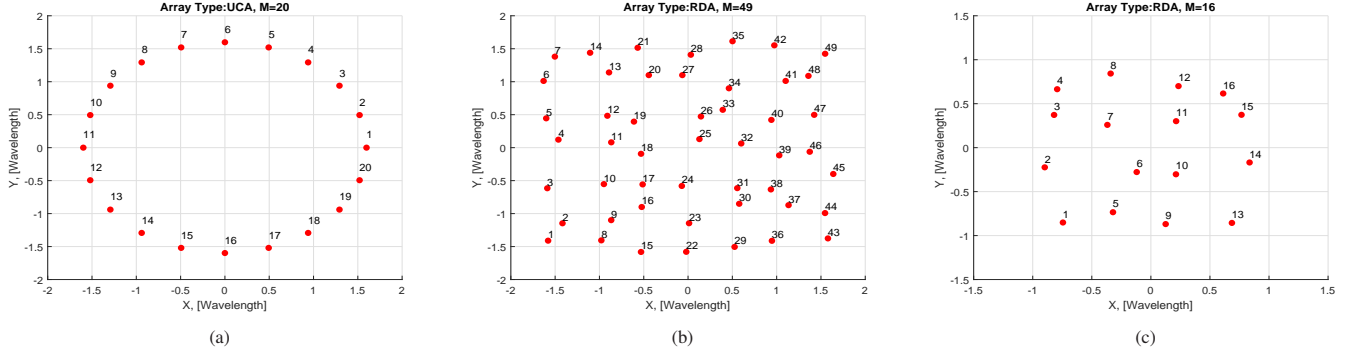


Fig. 3. The placement of antennas for a) UCA with $M = 20$ elements, b) RDA with $M = 49$ and c) RDA with $M = 16$.

Table 2 Selected antenna indices for UCA with $M = 16$ and $K \in \{3, 4, 5, 6, 7\}$, $\phi \in \{21.42^\circ, 74.28^\circ, 127.14^\circ, 232.85^\circ, 285.71^\circ\}$. The number of snapshots $L = 100$ and $\text{SNR}_{\text{TRAIN}} = 20\text{dB}$. The antennas are indexed counter-clockwise with the first antenna placed as shown in Fig. 3a.

	21.42°	74.28°	127.14°	232.85°	285.71°
K=3	{7, 17, 18}	{10, 11, 20}	{3, 13, 14}	{9, 18, 19}	{2, 11, 12}
K=4	{7, 8, 17, 18}	{1, 10, 11, 20}	{3, 4, 13, 14}	{8, 9, 18, 19}	{1, 2, 11, 12}
K=5	{7, 8, 16, 17, 18}	{1, 10, 11, 19, 20}	{3, 4, 12, 13, 14}	{8, 9, 10, 18, 19}	{1, 2, 11, 12, 13}
K=6	{6, 7, 8, 16, 17, 18}	{1, 9, 10, 11, 19, 20}	{2, 3, 4, 12, 13, 14}	{8, 9, 10, 18, 19, 20}	{1, 2, 3, 11, 12, 13}
K=7	{6, 7, 8, 16, 17, 18, 19}	{1, 9, 10, 11, 12, 19, 20}	{2, 3, 4, 5, 12, 13, 14}	{8, 9, 10, 17, 18, 19, 20}	{1, 2, 3, 11, 12, 13, 20}

wherein each element is chosen with approximately 10% selection rate. We provide the DoA estimation performance of the antenna subarrays selected by the network for different values of test data SNRs in the bottom plot of Fig. 2. We observe that, compared to our DL approach, the random thinning results in inferior DoA estimation due to small array aperture. Among various bounds, the MSE is somewhat similar at high SNR regimes with the BZB faring better than CRB at low SNRs.

4.2 2-D Arrays

We now investigate more complicated array geometries such as uniform circular arrays (UCAs) and randomly deployed arrays (RDAs). In Table 1, the computed values of Q and the reduced number of classes \bar{Q} are shown for UCAs with $M = 10$ and $M = 16$ elements where $P_\phi = 10000$ are uniformly spaced grid points in $[0^\circ, 360^\circ]$ and $\theta = 90^\circ$. We remark that the size of best subarray classes, \bar{Q} , is much less than Q .

4.2.1 Experiment #1: 1-D Scenario: We assume that the target and the antenna array are placed in the same plane (i.e., $\theta = 90^\circ$). We consider different array geometries such as UCAs and RDAs as shown in Figs. 3a and 3b, respectively. The UCAs consist of $M = 20$ and $M = 45$ elements where each antenna is placed half wavelength apart from each other. In order to generate the RDA geometry, we first take a uniform rectangular array of size 7×7 , and then perturb the antenna positions as $\{p_{x_m} + \delta_x, p_{y_m} + \delta_y\}_{m=1}^M$ where $\delta_x, \delta_y \sim \mathcal{U}[-0.1\lambda, 0.1\lambda]$.

The training set is constructed with $P_{\text{TRAIN}} = 100$ DoA angles. As an illustration of the training set generated, Table 2 lists the indices of a few UCA antennas that yield the best CRB for $M = 16$ and different target directions as K varies. We note that the subarrays that yield the largest aperture for the given target direction are selected due to the structure of UCA. The training samples are prepared for different SNR values (i.e., $\text{SNR}_{\text{TRAIN}}$) and the accuracy of training and validation phases is shown in Table 3.

In order to evaluate the classification performance of the proposed CNN structure, we fed the trained network with the test data generated with $L_{\text{TEST}} = 100$, $T_{\text{TEST}} = 100$ and $P_{\text{TEST}} = 100$ with $\phi_{\text{TEST}} \sim \mathcal{U}[[0^\circ, 360^\circ]]$. Figure 4 shows the classification performance of the CNN for $J_{\text{TEST}} = 100$ Monte Carlo trials. Figure 4 also shows the performance of the noisy test data when the network is trained with noise-free dataset; its performance degrades especially at low SNR levels. These observations imply that noisy

training datasets should be used for a robust classification performance with the test data. On the other hand, when the training data is corrupted with strong noise content (e.g., $\text{SNR}_{\text{TRAIN}} \leq 10\text{dB}$), then despite using the noisy training data, the proposed CNN does not recover from poor performance at low SNR_{TEST} regimes.

The performance at low SNRs can be improved when the size of the array increases and, as a result, the input data is huge and SNR is enhanced due to large M . As an example, Fig. 5 illustrates the performance of the network for UCA with $M = 45$ and $K = 5$, where the network provides high accuracy for a wide range of SNR_{TEST} compared to the scenario in Fig. 4.

We also compared CNN with the SVM technique (as in [34]) where we used identical parameters for the data generation and identical data covariance input to the SVM. The performance of SVM is shown in Fig. 6. We observe from Figs. 4-6 that CNN is more than 90% accurate for $\text{SNR}_{\text{TEST}} \geq 10\text{dB}$ when the network is trained by datasets with $\text{SNR}_{\text{TRAIN}} \geq 15\text{dB}$. In comparison, SVM performs poorly being unable to extract the features as efficiently as CNN.

Similar experimental results for an RDA (Fig. 3b) with $M = 49$ and $K = 5$ are shown in Fig. 7. The training dataset is prepared with the same parameters as in the previous experiment with UCA. For some selected cases, the accuracies of training and validation data for RDA are listed in Table 3. The network achieves high accuracy when M is large and $\text{SNR}_{\text{TEST}} \geq 10\text{dB}$.

4.2.2 Experiment #2: 2-D Scenario: Finally, we consider cases when the target and the antenna array are not coplanar. We train the CNN structure in Fig. 1 with the data generated for $T = 100$ and $L = 100$. The angles lies on a uniformly spaced elevation and azimuth grids in the planes $[90^\circ, 100^\circ]$ and $[0^\circ, 360^\circ]$, respectively. We set the number of grid points in the elevation and azimuth to $P_\theta = 11$ and $P_\phi = 100$, respectively.

In this experiment, we use an RDA (Fig. 3c) with $M = 16$ and $K = 6$. Table 4 lists the indices of a few RDA antennas that yield best CRB for different target DoAs: $\phi \in \{30^\circ, 60^\circ, 90^\circ, 120^\circ, 210^\circ\}$ and $\theta \in \{90^\circ, 92^\circ\}$ as K varies. When K increases, a subarray with larger aperture is to be selected for better DoA estimation performance. When there is even a slight change in the elevation angle, the best subarray changes completely because of the relatively small subarray aperture in the elevation dimension. We prepared the training and validation datasets for different $\text{SNR}_{\text{TRAIN}}$ values. The accuracies of the two stages are listed in Table 3. We note that the training accuracy of the network in the

Table 3 The accuracy percentages for training and validation datasets in 1-D and 2-D scenario.

SNR _{TRAIN}	1-D, UCA with $M = 20, K = 6$		1-D, UCA with $M = 45, K = 5$		1-D, RDA with $M = 49, K = 5$		2-D, RDA with $M = 16, K = 6$	
Training	Validation	Training	Validation	Training	Validation	Training	Validation	Training
10 dB	65.2%	68.7%	98.7%	97.8%	97.8%	95.7%	8.1%	10.7%
15 dB	98.1%	98.5%	99.0%	98.7%	99.9%	98.6%	60.1%	63.2%
20 dB	99.2%	99.5%	100%	99.7%	97.5%	98.1%	74.3%	74.4%
25 dB	99.4%	99.8%	100%	100%	100%	100%	80.1%	81.2%
30 dB	100%	100%	100%	100%	100%	100%	81.6%	80.9%
inf dB	100%	100%	100%	100%	100%	100%	88.9%	89.2%

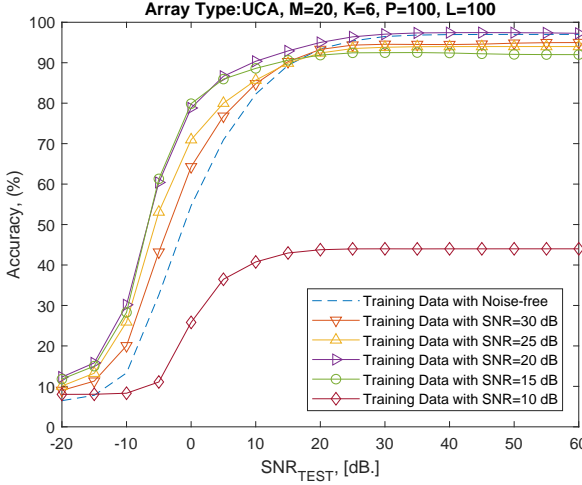


Fig. 4 Performance of test dataset using CNN with respect to SNR_{TEST} when the training data is prepared with $SNR_{TRAIN} \in \{10, 15, 20, 25, 30, \text{inf}\}$ dB. The antenna geometry is a UCA with $M = 20$ and $K = 6$.

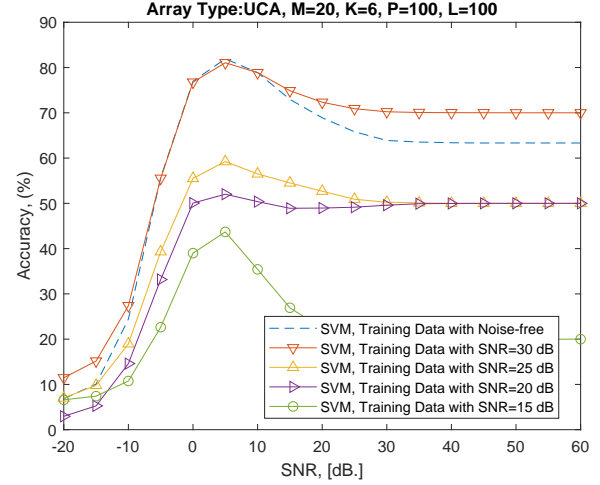


Fig. 6 Performance of test dataset using SVM with respect to SNR_{TEST} when the training data is prepared with $SNR_{TRAIN} \in \{10, 15, 20, 25, 30, \text{inf}\}$ dB. The antenna geometry is a UCA with $M = 20$ and $K = 6$.

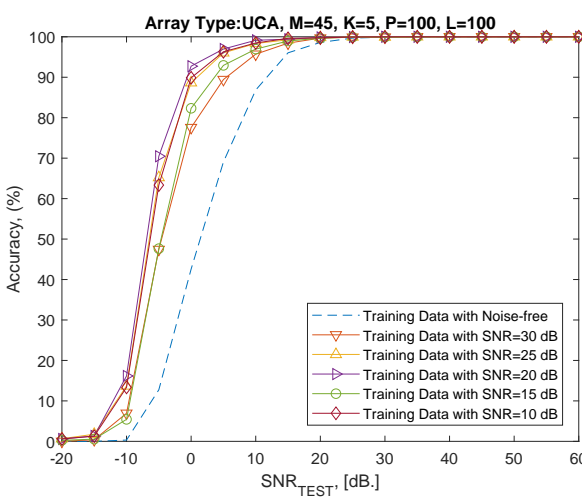


Fig. 5 Performance of test data using CNN with respect to SNR when the training data is prepared with $SNR_{TRAIN} \in \{10, 15, 20, 25, 30, \text{inf}\}$ dB. The antenna geometry is a UCA with $M = 45$ and $K = 5$.

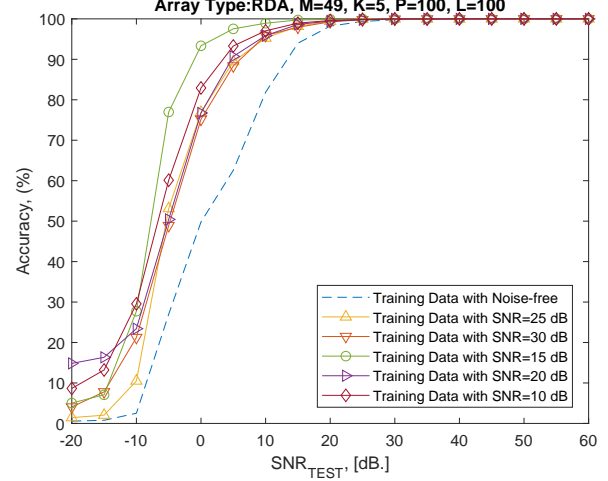


Fig. 7 Performance of test data using CNN with respect to SNR when the training data is prepared with $SNR_{TRAIN} \in \{5, 10, 15, 20, 25, 30, \text{inf}\}$ dB. The antenna geometry is an RDA with $M = 49$ shown in Fig. 3b and $K = 5$.

2-D case is worse than the 1-D scenario of RDA because simple 2-D arrays are unable to distinguish all elevation angles. This leads to the training data samples, that are labeled to different classes with different elevation angles, very similar to each other.

We generated a test dataset with $L_{TEST} = 100$ and $T_{TEST} = 100$ to evaluate the CNN for a 2-D target scenario. The target directions were drawn from $\phi_{TEST} \sim u\{[0^\circ, 360^\circ]\}$ and $\theta_{TEST} \sim u\{[80^\circ, 100^\circ]\}$ for $P_{TEST} = 100$. The accuracies of the test mode for $J_{TEST} = 100$ trials is shown in Fig. 8 for different SNR_{TEST} levels. Figure 8 shows that the training datasets with $SNR_{TRAIN} \geq 15$ dB provide sufficiently good performance with an accuracy of

approximately 85% for $SNR_{TEST} \geq 10$ dB. However, as seen earlier, poor classification performance results when SNR_{TRAIN} is low (e.g., ≤ 10 dB).

5 Discussion and Summary

We introduced a method based on DL to select antennas in a cognitive radar scenario. We constructed a deep neural network with convolutional layers as a multi-class classification framework. The training data was generated such that each class indicated an antenna subarray that provides the lowest minimal error bound for estimating

Table 4 Selected antenna indices for random array with $M = 16$ and $K \in \{3, 4, 5, 6, 7\}$, $\phi \in \{30^\circ, 60^\circ, 90^\circ, 120^\circ, 210^\circ\}$ and $\theta \in \{90^\circ, 92^\circ\}$. The number of snapshots $L = 100$ and $\text{SNR}_{\text{TRAIN}}=20\text{dB}$. Note that the antenna indices are given in Fig. 3c.

	$\theta = 90^\circ, \phi = 30^\circ$	$\theta = 90^\circ, \phi = 60^\circ$	$\theta = 90^\circ, \phi = 90^\circ$	$\theta = 90^\circ, \phi = 120^\circ$	$\theta = 90^\circ, \phi = 210^\circ$
K=3	{4, 8, 13}	{3, 4, 13}	{2, 14, 15}	{1, 15, 16}	{4, 8, 13}
K=4	{4, 8, 9, 13}	{3, 4, 13, 14}	{2, 3, 14, 15}	{1, 2, 15, 16}	{4, 8, 9, 13}
K=5	{3, 4, 8, 9, 13}	{3, 4, 8, 13, 14}	{2, 3, 4, 14, 15}	{1, 2, 14, 15, 16}	{2, 3, 4, 14, 15}
K=6	{3, 4, 8, 9, 13, 14}	{3, 4, 8, 9, 13, 14}	{2, 3, 4, 13, 14, 15}	{1, 2, 5, 14, 15, 16}	{3, 4, 8, 9, 13, 14}
K=7	{3, 4, 5, 8, 9, 13, 14}	{2, 3, 4, 8, 9, 13, 14}	{1, 2, 3, 4, 13, 14, 15}	{1, 2, 5, 12, 14, 15, 16}	{1, 2, 3, 4, 13, 14, 15}
	$\theta = 92^\circ, \phi = 30^\circ$	$\theta = 92^\circ, \phi = 60^\circ$	$\theta = 92^\circ, \phi = 90^\circ$	$\theta = 92^\circ, \phi = 120^\circ$	$\theta = 92^\circ, \phi = 210^\circ$
K=3	{1, 2, 15}	{1, 8, 16}	{1, 8, 9}	{4, 12, 13}	{1, 2, 15}
K=4	{1, 2, 14, 16}	{1, 9, 12, 16}	{1, 8, 12, 13}	{4, 8, 9, 13}	{1, 2, 14, 16}
K=5	{1, 2, 14, 15, 16}	{1, 5, 8, 12, 16}	{1, 8, 9, 12, 13}	{4, 8, 9, 12, 13}	{1, 2, 14, 15, 16}
K=6	{1, 2, 5, 14, 15, 16}	{1, 5, 9, 12, 15, 16}	{1, 8, 9, 12, 13, 16}	{3, 4, 5, 8, 9, 13}	{1, 8, 9, 12, 13, 16}
K=7	{1, 2, 3, 5, 14, 15, 16}	{1, 5, 8, 9, 12, 15, 16}	{1, 4, 8, 9, 12, 13, 16}	{3, 4, 5, 8, 9, 12, 13}	{1, 2, 3, 5, 14, 15, 16}

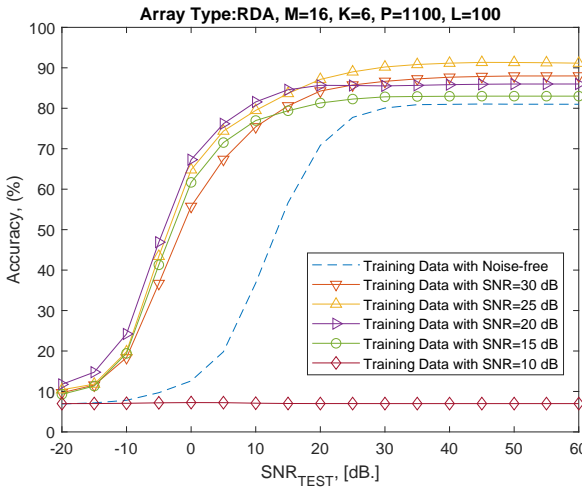


Fig. 8 Performance of test data using CNN with respect to SNR when the training data is prepared with $\text{SNR}_{\text{TRAIN}} \in \{5, 10, 15, 20, 25, 30, \text{inf}\}$ dB. The antenna geometry is an RDA with $M = 16$ shown in Fig. 3c and $K = 6$.

target DoA in a given scenario. Our learning network then cognitively determines a new array whenever the radar receiver acquires echoes from the target scene. We evaluated the performance of the proposed approach for both 1-D (azimuth) and 2-D (azimuth and elevation) target scenarios using ULA, UCA and RDA structures. The results show enhanced performance of the proposed network over conventional randomly thinned arrays as well as the traditional SVM-based selection. Our method does not have dependence on the array geometry and selects optimal antenna subarrays for DoA estimation. We remark that the classification accuracy of the CNN degrades in low SNR conditions because the network cannot distinguish the array data of different classes and, consequently, predicts false results. We were able to partially mitigate this issue by training the network with noisy data samples.

Although the CNN predicts an optimal subarray for 1-D scenarios very well, its performance diminishes for 2-D cases. This is expected because the simple 2-D arrays we considered are unable to distinguish all elevation angles and thereby lead to some misclassification. We reserve further investigations on this issue for the future.

Acknowledgment

K.V.M. acknowledges partial support via Andrew and Erna Finci Viterbi Fellowship and Lady Davis Fellowship.

6 References

1. S. Haykin, "Cognitive radar: A way of the future," *IEEE Signal Processing Magazine*, vol. 23, no. 1, pp. 30–40, 2006.

2. J. R. Guerci, "Cognitive radar: A knowledge-aided fully adaptive approach," in *IEEE Radar Conference*, pp. 1365–1370, 2010.
3. G. E. Smith, Z. Cammenga, A. Mitchell, K. L. Bell, J. Johnson, M. Rangaswamy, and C. Baker, "Experiments with cognitive radar," *IEEE Aerospace and Electronic Systems Magazine*, vol. 31, no. 12, pp. 34–46, 2016.
4. P. Chen and L. Wu, "Waveform design for multiple extended targets in temporally correlated cognitive radar system," *IET Radar, Sonar & Navigation*, vol. 10, no. 2, pp. 398–410, 2016.
5. M. B. Kilani, Y. Nijssure, G. Gagnon, G. Kaddoum, and F. Gagnon, "Cognitive waveform and receiver selection mechanism for multistatic radar," *IET Radar, Sonar & Navigation*, vol. 10, no. 2, pp. 417–425, 2016.
6. K. V. Mishra and Y. C. Eldar, "Performance of time delay estimation in a cognitive radar," in *IEEE International Conference on Acoustics, Speech and Signal Processing*, pp. 3141–3145, 2017.
7. K. V. Mishra, E. Shoshan, M. Namer, M. Meltsin, D. Cohen, R. Madmoni, S. Dror, R. Ifraimov, and Y. C. Eldar, "Cognitive sub-Nyquist hardware prototype of a collocated MIMO radar," in *International Workshop on Compressed Sensing Theory and its Applications to Radar, Sonar and Remote Sensing*, pp. 56–60, 2016.
8. K. L. Bell, C. J. Baker, G. E. Smith, J. T. Johnson, and M. Rangaswamy, "Cognitive radar framework for target detection and tracking," *IEEE Journal of Selected Topics in Signal Processing*, vol. 9, no. 8, pp. 1427–1439, 2015.
9. N. A. Goodman, P. R. Venkata, and M. A. Neifeld, "Adaptive waveform design and sequential hypothesis testing for target recognition with active sensors," *IEEE Journal of Selected Topics in Signal Processing*, vol. 1, no. 1, pp. 105–113, 2007.
10. P. Stinco, M. S. Greco, and F. Gini, "Spectrum sensing and sharing for cognitive radars," *IET Radar, Sonar & Navigation*, vol. 10, no. 3, pp. 595–602, 2016.
11. D. Cohen, K. V. Mishra, and Y. C. Eldar, "Spectrum sharing radar: Coexistence via Xampling," *IEEE Transactions on Aerospace and Electronic Systems*, 2017, in press.
12. C. Baylis, M. Fellows, L. Cohen, and R. J. M. II, "Solving the spectrum crisis: Intelligent, reconfigurable microwave transmitter amplifiers for cognitive radar," *IEEE Microware Magazine*, vol. 15, no. 5, pp. 94–107, 2014.
13. Y. Lo, "A mathematical theory of antenna arrays with randomly spaced elements," *IEEE Transactions on Antennas and Propagation*, vol. 12, no. 3, pp. 257–268, 1964.
14. T. M. Duman and A. Ghayeb, "Antenna selection for MIMO systems," in *Coding for MIMO Communication Systems*, pp. 287–315, John Wiley & Sons, 2007.
15. A. Gershman and J. F. Böhme, "A note on most favorable array geometries for DOA estimation and array interpolation," *IEEE Signal Processing Letters*, vol. 4, no. 8, pp. 232–235, 1997.
16. P. Pal and P. P. Vaidyanathan, "Coprime sampling and the MUSIC algorithm," in *Digital Signal Processing and Signal Processing Education Meeting*, pp. 289–294, 2011.
17. P. Pal and P. P. Vaidyanathan, "Nested arrays: A novel approach to array processing with enhanced degrees of freedom," *IEEE Transactions on Signal Processing*, vol. 58, no. 8, pp. 4167–4181, 2010.
18. K. V. Mishra, I. Kahane, A. Kaufmann, and Y. C. Eldar, "High spatial resolution radar using thinned arrays," in *IEEE Radar Conference*, pp. 1119–1124, 2017.
19. M. Rossi, A. M. Haimovich, and Y. C. Eldar, "Spatial compressive sensing for MIMO radar," *IEEE Transactions on Signal Processing*, vol. 62, no. 2, pp. 419–430, 2014.
20. J. Tabrikian, O. Isaacs, and I. Bilik, "Cognitive antenna selection for DOA estimation in automotive radar," in *IEEE Radar Conference*, pp. 1–5, 2016.
21. O. Isaacs, J. Tabrikian, and I. Bilik, "Cognitive antenna selection for optimal source localization," in *IEEE International Workshop on Computational Advances in Multi-Sensor Adaptive Processing*, pp. 341–344, 2015.
22. G. Shulkind, S. Jegelka, and G. W. Wornell, "Multiple wavelength sensing array design," in *IEEE International Conference on Acoustics, Speech and Signal Processing*, pp. 3424–3428, 2017.
23. H. Nosrati, E. Aboutanios, and D. B. Smith, "Receiver-transmitter pair selection in MIMO phased array radar," in *IEEE International Conference on Acoustics, Speech and Signal Processing*, pp. 3206–3210, 2017.
24. A. F. Molisch, V. V. Ratnam, S. Han, Z. Li, S. L. H. Nguyen, L. Li, and K. Haneda, "Hybrid beamforming for massive MIMO: A survey," *IEEE Communications Magazine*, vol. 55, no. 9, pp. 134–141, 2017.
25. X. Zhai, Y. Cai, Q. Shi, M. Zhao, G. Y. Li, and B. Champagne, "Joint transceiver design with antenna selection for large-scale MU-MIMO mmWave systems," *IEEE Journal on Selected Areas in Communications*, vol. 35, no. 9, pp. 2085–2096, 2017.

26 Z. Wang and L. Vandendorpe, "Antenna selection for energy efficient MISO systems," *IEEE Communications Letters*, 2017. in press.

27 O. T. Demir and T. E. Tuncer, "Antenna selection and hybrid beamforming for simultaneous wireless information and power transfer in multi-group multicasting systems," *IEEE Transactions on Wireless Communications*, vol. 15, no. 10, pp. 6948–6962, 2016.

28 S. Joshi and S. Boyd, "Sensor selection via convex optimization," *IEEE Transactions on Signal Processing*, vol. 57, no. 2, pp. 451–462, 2009.

29 V. Roy, S. P. Chepuri, and G. Leus, "Sparsity-enforcing sensor selection for DOA estimation," in *IEEE International Workshop on Computational Advances in Multi-Sensor Adaptive Processing*, pp. 340–343, 2013.

30 H. Godrich, A. P. Petropulu, and H. V. Poor, "Sensor selection in distributed multiple-radar architectures for localization: A knapsack problem formulation," *IEEE Transactions on Signal Processing*, vol. 60, no. 1, pp. 247–260, 2012.

31 J. Metcalf, S. D. Blunt, and B. Himed, "A machine learning approach to cognitive radar detection," in *IEEE Radar Conference*, pp. 1405–1411, 2015.

32 Y. Gao, D. Hu, Y. Chen, and Y. Ma, "Gridless 1-b DOA estimation exploiting SVM approach," *IEEE Communications Letters*, vol. 21, no. 10, pp. 2210–2213, 2017.

33 A. E. Gonnouni, M. Martinez-Ramon, J. L. Rojo-Alvarez, G. Camps-Valls, A. R. Figueiras-Vidal, and C. G. Christodoulou, "A support vector machine MUSIC algorithm," *IEEE Transactions on Antennas and Propagation*, vol. 60, no. 10, pp. 4901–4910, 2012.

34 J. Joung, "Machine learning-based antenna selection in wireless communications," *IEEE Communications Letters*, vol. 20, no. 11, pp. 2241–2244, 2016.

35 Y. LeCun, Y. Bengio, and G. Hinton, "Deep learning," *Nature*, vol. 521, no. 7553, pp. 436–444, 2015.

36 Y. Bengio, A. Courville, and P. Vincent, "Representation learning: A review and new perspectives," *IEEE Transactions on Pattern Analysis and Machine Intelligence*, vol. 35, no. 8, pp. 1798–1828, 2013.

37 C. Wang, J. Wang, and X. Zhang, "Automatic radar waveform recognition based on time-frequency analysis and convolutional neural network," in *IEEE International Conference on Acoustics, Speech and Signal Processing*, pp. 2437–2441, 2017.

38 E. Mason, B. Yonet, and B. Yazici, "Deep learning for radar," in *IEEE Radar Conference*, pp. 1703–1708, 2017.

39 C. P. Schwegmann, W. Kleynhans, B. P. Salmon, L. W. Mdakane, and R. G. V. Meyer, "Very deep learning for ship discrimination in Synthetic Aperture Radar imagery," in *IEEE International Geoscience and Remote Sensing Symposium*, pp. 104–107, 2016.

40 B. Jokanović and M. Amin, "Fall detection using deep learning in range-Doppler radars," *IEEE Transactions on Aerospace and Electronic Systems*, 2017. in press.

41 A. Renaux, P. Forster, P. Larzabal, C. D. Richmond, and A. Nehorai, "A fresh look at the Bayesian bounds of the Weiss-Weinstein family," *IEEE Transactions on Signal Processing*, vol. 56, no. 11, pp. 5334–5352, 2008.

42 T. Jiang, N. D. Sidiropoulos, and J. M. ten Berge, "Almost-sure identifiability of multidimensional harmonic retrieval," *IEEE Transactions on Signal Processing*, vol. 49, no. 9, pp. 1849–1859, 2001.

43 X. Liu and N. D. Sidiropoulos, "On constant modulus multidimensional harmonic retrieval," in *IEEE International Conference on Acoustics, Speech, and Signal Processing*, vol. 3, pp. III–2977, 2002.

44 D. Nion and N. D. Sidiropoulos, "Tensor algebra and multidimensional harmonic retrieval in signal processing for MIMO radar," *IEEE Transactions on Signal Processing*, vol. 58, no. 11, pp. 5693–5705, 2010.

45 Z. Ben-Haim and Y. C. Eldar, "A lower bound on the Bayesian MSE based on the optimal bias function," *IEEE Transactions on Information Theory*, vol. 55, no. 11, pp. 5179–5196, 2009.

46 P. Stoica and A. Nehorai, "MUSIC, maximum likelihood, and Cramér-Rao bound: Further results and comparisons," *IEEE Transactions on Acoustics, Speech, and Signal Processing*, vol. 38, no. 12, pp. 2140–2150, 1990.

47 B. Friedlander and A. Weiss, "Direction finding in the presence of mutual coupling," *IEEE Transactions on Antennas and Propagation*, vol. 39, no. 3, pp. 273–284, 1991.

48 Z. Ye and C. Liu, "2-D DOA estimation in the presence of mutual coupling," *IEEE Transactions on Antennas and Propagation*, vol. 56, no. 10, pp. 3150–3158, 2008.

49 N. Srivastava, G. Hinton, A. Krizhevsky, I. Sutskever, and R. Salakhutdinov, "Dropout: A simple way to prevent neural networks from overfitting," *Journal of Machine Learning Research*, vol. 15, no. 1, pp. 1929–1958, 2014.

50 C. M. Bishop, *Pattern Recognition and Machine Learning*. Springer, New York, 2006.